

Imaging of short-wavelength spin waves in a nanometer-thick YIG/Co bilayer

Abhishek Talapatra,¹ Huajun Qin,^{2,3,*} Frank Schulz,⁴ Lide Yao,¹ Lukáš Flajšman,¹ Markus Weigand,⁵ Sebastian Wintz,⁴ and Sebastiaan van Dijken^{1,*}

¹*Department of Applied Physics, Aalto University School of Science, FI-00076 Aalto, Finland*

²*School of Physics and Technology, Wuhan University, Wuhan 430072, China*

³*Wuhan Institute of Quantum Technology, Wuhan 430206, China*

⁴*Max Planck Institute for Intelligent Systems, 70569 Stuttgart, Germany*

⁵*Helmholtz-Zentrum Berlin für Materialien und Energie GmbH, 14109 Berlin, Germany*

We report the imaging of short-wavelength spin waves in a continuous nanometer-thick YIG film with a Co stripe patterned on top. Dynamic dipolar coupling between the YIG film and the Co stripe lowers the spin-wave wavelength when spin waves enter the YIG/Co bilayer region from the bare YIG film, causing partial reflection at the YIG/Co edge. We use time-resolved scanning transmission X-ray microscopy to image the mode conversion process down to a wavelength of 280 nm and extract the spin-wave dispersion, decay length and magnetic damping in the YIG/Co bilayer. We also analyze spin-wave reflection from the YIG/Co edge and its dependence on the wavelength of incoming and transmitted spin waves.

Scalable magnonics utilizing short-wavelength spin waves as information carriers is of great interest for parallel wave-based logic and unconventional computing^{1–4}. Most magnonic devices demonstrated thus far, including logic gates^{5,6}, transistors⁷, multiplexers⁸, and directional couplers^{9,10} utilize long-wavelength dipolar spin waves. To scale down the size of computing units, speed up information processing, and realize complex magnonic circuitry, it is essential to exploit shorter dipole-exchange or exchange spin waves at technologically relevant frequencies ranging from a few to tens of GHz. Microwave antennas are not suitable for short-wave excitation in the linear regime. As good alternatives, coherent emission of dipole-exchange spin waves from noncollinear spin textures^{11–15}, magnetic nanostructure edges^{16,17}, thickness steps¹⁸, magnonic bilayers¹⁹, and magnetic interfaces^{20–22} under uniform microwave irradiation has been demonstrated. Moreover, for ferrimagnetic yttrium iron garnet (YIG) films with ultralow Gilbert damping, the excitation of short-wavelength propagating waves through a grating coupler (ferromagnetic (FM) dot or stripe array)^{23–26} or a magnetic coplanar waveguide²⁷ is attractive. Grating couplers acting as microwave-to-magnon transducers^{28,29} provide non-reciprocal spin-wave emission because of chiral dipolar coupling between FM nanostructures and a YIG film near the ferromagnetic resonance (FMR) frequency of the FM³⁰. Recently, we demonstrated a magnonic Fabry-Pérot resonator made from a YIG film and a single FM nanostripe³¹. In this hybrid structure, the wavelength of incoming spin waves downconverts in the bilayer. Analogous to an optical Fabry-Pérot resonator, destructive interference of the spin waves entering and the spin waves circulating the YIG/FM bilayer produces clear transmission gaps at discrete frequencies. In the

magnonic version, the wavelength of spin waves propagating in opposite directions is different because of the chirality of dipolar coupling. One of the wavelengths is much shorter than that of the incoming spin waves, facilitating significant downscaling for programmable control of spin waves on the nanoscale. Moreover, for larger stripe widths, the bilayer acts as a magnonic diode because the counterpropagating waves damp out differently. The magnonic Fabry-Pérot resonator enables manipulation of spin-wave signals well below the FMR frequency of the FM.

Here, we investigate spin-wave mode conversion and reflection at the edge of a YIG/FM bilayer. In our experiments, we consider continuous YIG films with Co stripes patterned on top. Because the short-wavelength propagating mode inside the bilayer could not be resolved by super-Nyquist sampling magneto-optical Kerr effect microscopy, as was used in our previous work³¹, we now image the spin waves by time-resolved scanning transmission X-ray microscopy (TR-STXM)^{32–35}. From the data, we extract the spin-wave dispersion, decay length, damping parameter, and reflection coefficient. Our results demonstrate a simple and efficient method for generating short-wavelength spin waves.

The YIG film with a thickness of 52 nm was grown on a (111)-oriented Gd₃Ga₅O₁₂ (GGG) substrate by pulsed laser deposition (PLD) at 800°C in 0.13 mbar oxygen^{36,37}. We used an excimer laser with a pulse repetition rate of 2 Hz and a laser fluence of 1.8 J/cm². After growth, the YIG film was annealed at 730°C for 10 minutes in 13 mbar oxygen before slow cooling down to room temperature. On top of the YIG film, 30-nm-thick Co stripes were patterned using direct laser writing lithography and lift-off. The Co stripes are separated from the YIG film by a 3 nm TaO_x spacer to eliminate interface exchange coupling, i.e., the two magnetic layers couple via dynamic dipolar fields only. Near the Co stripes, we patterned 2-μm-wide microwave antennas out of a 3 nm Ta/150 nm Au stack. Next, we opened several windows for STXM measurements in areas with a Co stripe, close to a microwave

*Authors to whom correspondence should be addressed: qinhua-jun@whu.edu.cn and sebastiaan.van.dijken@aalto.fi

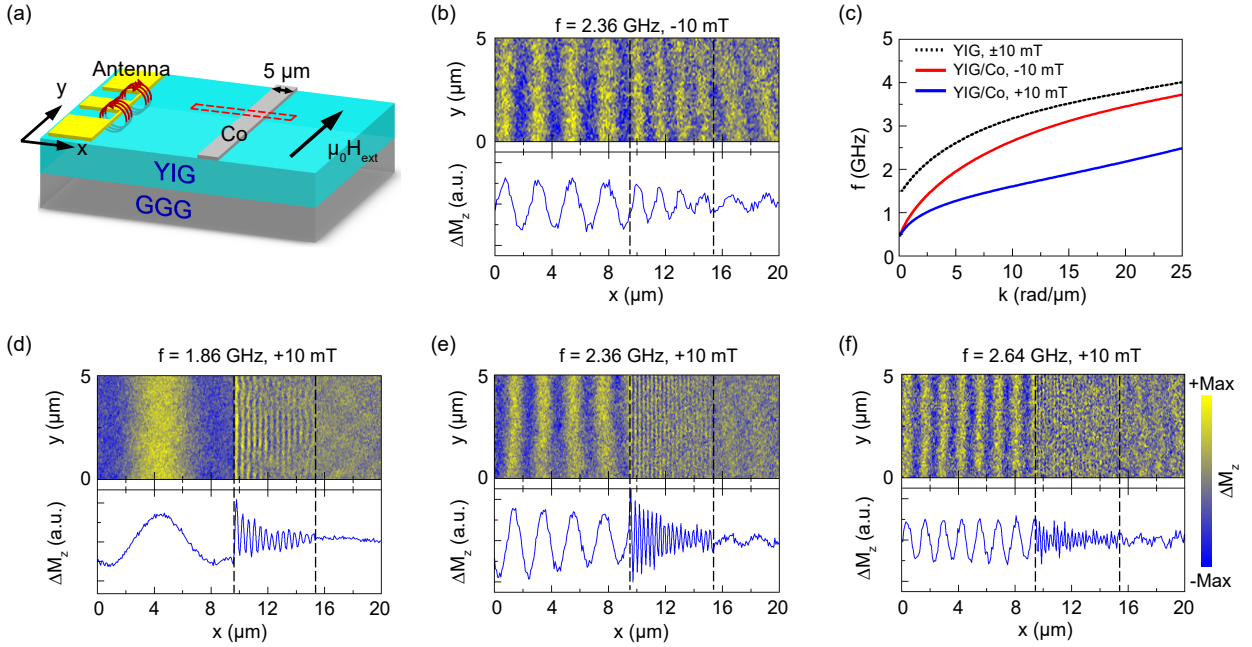


FIG. 1. (a) Schematic of the measurement geometry. The device consists of a $5\ \mu\text{m}$ -wide Co stripe patterned on top of a 52-nm-thick YIG film. A $2\ \mu\text{m}$ -wide microwave antenna made of 3 nm Ta/150 nm Au is patterned on the YIG film $30\ \mu\text{m}$ away from the Co stripe. The dashed box indicates the field of view of the STXM measurements. The arrow indicates the direction of positive applied magnetic field. (b) Normalized TR-STXM image (snapshot in time) of a propagating spin wave and the corresponding line profile recorded at 2.36 GHz and $-10\ \text{mT}$. The dashed lines mark the two edges of the Co stripe. (c) Calculated spin-wave dispersions for the bare YIG film (black dashed line) and the YIG/Co bilayer (red and blue solid lines) for $\pm 10\ \text{mT}$. (d-f) Normalized TR-STXM images of propagating spin waves and corresponding line profiles recorded at 1.86 GHz, 2.36 GHz, and 2.64 GHz with a $+10\ \text{mT}$ bias field.

antenna. To do this, we mounted the sample on a Cu ring and mechanically polished the GGG substrate from the backside to a thickness of about $25\ \mu\text{m}$. Hereafter, we used focused ion beam (FIB, JEOL JIB 4700F) milling to open $40\ \mu\text{m} \times 40\ \mu\text{m}$ windows with a thickness of $\sim 250\ \text{nm}$. STXM measurements were carried out at the Maxymus endstation at the BessyII electron storage ring operated by the Helmholtz-Zentrum Berlin für Materialien und Energie. In the STXM experiments, we used circularly polarized X-rays with an energy of nominally 710.4 eV (L_3 resonant X-ray absorption edge of Fe) to image propagating spin waves in the YIG film through the X-ray magnetic circular dichroism (XMCD) effect, exploiting the central dichroic peak of YIG³⁸.

Figure 1(a) illustrates the sample structure with a $5\text{-}\mu\text{m}$ -wide Co stripe on top of the YIG film. The distance between the Co stripe and the microwave antenna is $30\ \mu\text{m}$. An external magnetic field of $\mu_0 H_{\text{ext}} = \pm 10\ \text{mT}$ is applied along the antenna to saturate the magnetization of the YIG film and the Co stripe for spin-wave characterization in the Damon-Eshbach (DE) geometry. TR-STXM measurements are conducted in the area marked by a red dashed box in Fig. 1(a). Because the measurement energy is set to the L_3 X-ray absorption edge of Fe, we only image the magnetization dynamics in YIG. To perform 2D scans of propagating spin waves, the sample stage was moved in steps of $75\ \text{nm}$ along the x

and y directions. Figure 1(b) shows the result for an excitation frequency of 2.36 GHz and a bias field of $-10\ \text{mT}$. The image shows an instant snapshot of the perpendicular magnetization component as normalized to the time average state. In this magnetic configuration, the spin wave propagating from the microwave antenna to the Co stripe shortens slightly upon entering the YIG/Co bilayer (first dashed line). This mode conversion effect is illustrated more clearly by the line profile shown in the lower panel of Fig. 1(b), obtained by averaging the 2D data along the y axis. When leaving the bilayer region (second dashed line), the spin wave retains its original wavelength. Mode conversion is explained by a frequency downshift (or equivalently wavenumber increase) of the spin-wave dispersion in the YIG/Co bilayer compared to that of the uncovered YIG film (Fig. 1(c)). Figure 1(c) presents the spin-wave dispersions in the YIG/Co bilayer (red and blue solid lines) and in the bare YIG film (black dashed line) for $\pm 10\ \text{mT}$, which we calculated using Grünberg's model³⁹ and the Kalinikos and Slavin formula⁴⁰, respectively. To account for the dipole-exchange character of spin waves in the YIG/Co bilayer, the intralayer exchange terms for individual Co and YIG layers were added to the Grünberg model by substituting $H \rightarrow H_{\text{ext}} + 2A_{\text{ex}}/(\mu_0 M_s)k_z^{2,31}$. Here, A_{ex} and M_s are the exchange constant and saturation magnetization of the Co and YIG layer. The interlayer exchange coupling is assumed to be

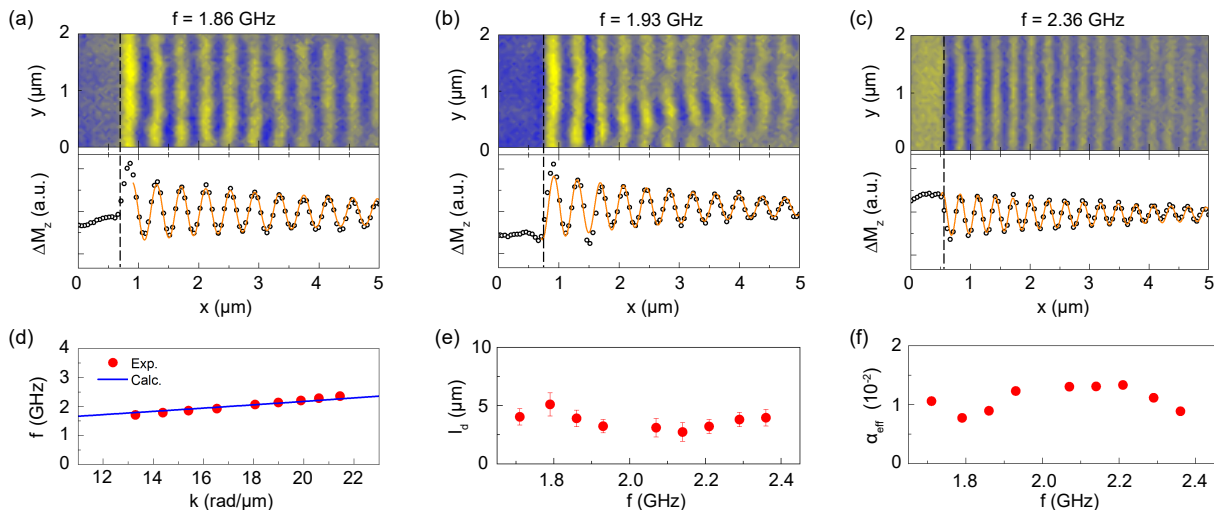


FIG. 2. (a-c) High-resolution normalized TR-STXM images and line profiles of propagating short-wavelength spin waves in the YIG/Co bilayer at 1.86 GHz, 1.93 GHz, and 2.35 GHz with a +10 mT bias field. The line profiles are obtained by averaging the measurement data along the y axis. The dashed lines mark the edge of the Co stripe. The orange line is a fit to the data using a damped sine wave (see text). (d-f) Measured (symbol) and calculated (line) spin-wave dispersion (d), decay length (e), and effective magnetic damping constant (f).

zero because of the 3-nm-thick TaO_x spacer between the YIG and Co layers. Obviously, the spin-wave dispersion of the YIG/Co bilayer is different from that of the bare YIG film at ± 10 mT. In YIG/Co, the spin-wave frequency softens slightly for -10 mT (red solid line), while it reduces significantly for $+10$ mT (blue solid line), compared to the dispersion in YIG. The strong dependence of the spin-wave dispersion in YIG/Co on the direction of external magnetic field (or magnetization) stems from the chirality of the dynamic dipolar coupling between the YIG and Co layers²⁹⁻³¹. Because of the dispersion shift, the wavelength of spin waves converts down upon entering the YIG/Co bilayer and it reverts back up when the spin waves leave the bilayer region, as seen in Fig. 1(b) for -10 mT. Figure 1(d-f) depicts normalized TR-STXM images of spin-wave propagation across the YIG/Co bilayer, recorded at three different excitation frequencies and a bias field of $+10$ mT. The selected frequencies represent a low, middle and high frequency within the excitation range of the microwave antenna at this field. Now, the wavelength of the spin waves reduces by more than an order of magnitude within the YIG/Co bilayer, again in agreement with the dispersion calculations in Fig. 1(c). The conversion efficiency is rather high as the amplitude of short-wavelength spin waves near the YIG/Co bilayer edge is comparable (or even larger) than that of the long-wavelength spin waves in the uncovered YIG film, indicating an efficient way to excite short-wavelength spin waves in hybrid magnonic structures. The conversion of energy at the injection/reflection boundary depends on wave localization and wave ellipticity. The long-wavelength spin waves in the YIG film are elliptical along x and nearly uniform across the film thickness, while the short-wavelength spin waves in the YIG film of the YIG/Co bilayer are elliptical along z and localized near the top surface³¹.

To analyze the propagation of short-wavelength spin waves

further, we performed high-resolution STXM imaging in the frequency range from 1.79 to 2.28 GHz (Fig. 2 (a-c)). The 2D images were recorded in a $2 \mu\text{m} \times 5 \mu\text{m}$ window that mainly covered the YIG/Co bilayer by moving the sample stage in steps of 50 nm along the x and y directions. Corresponding line profiles representing the averaged spin-wave signal along the y axis in the normalized TR-STXM images are shown in the lower panels of Fig. 2(a-c). We extracted the spin-wave wavelength λ and decay length l_d in the YIG/Co bilayer by fitting the data using $y = A \exp(-x/l_d) \sin(2\pi x/\lambda + \phi)$. The measured bilayer dispersion for short-wavelength spin waves is depicted in Fig. 2(d), together with a calculation based on the Grünberg model³⁹. The wavelength decreases from 480 nm at 1.79 GHz to 280 nm at 2.28 GHz. Figure 2(e) shows the decay length of the spin waves in the YIG/Co bilayer as a function of frequency. The decay length is about $4 \mu\text{m}$, which is much shorter than the decay length of the dipolar spin waves in the uncovered YIG film ($l_d \approx 20 \mu\text{m}$). The decay length depends only weakly on frequency. This is explained by a nearly constant spin-wave group velocity in the measured frequency range, as illustrated by the close to linear spin-wave dispersion in Fig. 2(d). The decay length in YIG/Co is also small compared to the YIG/CoFeB Fabry-Pérot resonators we studied previously³¹. For YIG/CoFeB, we estimated $l_d \approx 10 \mu\text{m}$ from the magnonic diode effect in μm -wide stripes. The smaller spin-wave decay length in our current experiments is explained by stronger magnetic damping in Co compared to CoFeB (see below) and the use of a thinner YIG film with lower group velocity (52 nm instead of 100 nm). To extract the effective magnetic damping (α) in YIG/Co, we derived the spin-wave group velocity from the dispersion curve. Using $\alpha_{eff} = \frac{v_g}{2\pi l_d f}$ ³⁶, we obtained $\alpha_{eff} \approx 0.01$ in the measured frequency range (Fig. 2(f)).

We conducted FMR measurements on a continuous

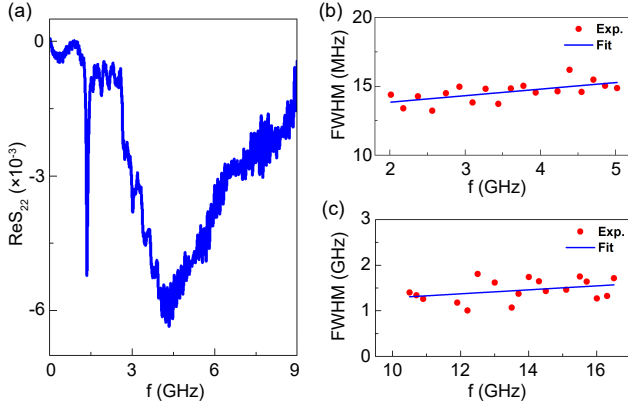


FIG. 3. (a) Real part of the S_{22} scattering parameter measured on a YIG/Co bilayer at +10 mT. (b,c) Linewidth of the FMR mode in the YIG (b) and Co (c) layer as a function of frequency. The line is a linear fit to the data.

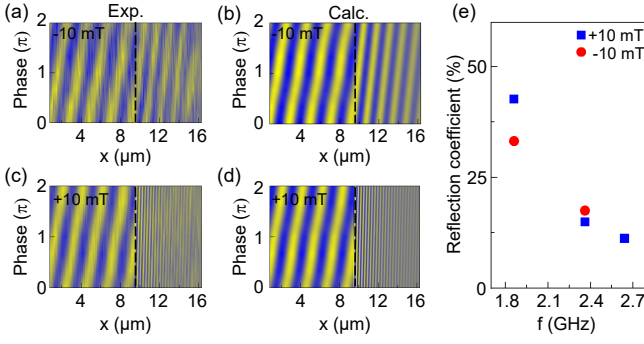


FIG. 4. (a,b) Measured phase-resolved TR-STXM data (a) and calculated profiles of the spin-wave phase (b) at 2.36 GHz and -10 mT. (c,d) Analogous data as in (a,b), but for a magnetic bias field of $+10$ mT. (e) Determined spin-wave reflection coefficient of the YIG/Co bilayer edge as a function of frequency.

YIG/Co bilayer using a coplanar waveguide to investigate the magnetic damping in the YIG and Co layers. Figure 3(a) shows the real part of scattering parameter S_{22} as a function of frequency, recorded in a $+10$ mT bias field. The sharp resonance around 1.4 GHz corresponds to the FMR mode in the YIG film and the broad resonance at 4.3 GHz is produced by the FMR mode in Co. By measuring FMR spectra at different bias fields, we extracted plots of the FMR linewidth versus frequency for YIG and Co (Fig. 3(b,c)). Fitting the data to $\Delta f = 2\alpha f + \text{const.}$, gives $\alpha_{\text{YIG}} = 5 \times 10^{-4}$ for YIG and $\alpha_{\text{Co}} = 0.04$ for Co. This result clearly indicates that dynamic dipolar coupling of propagating spin waves in YIG to the strongly damped Co layer limits the decay length of the short-wavelength spin waves. To realize longer-distance transport of dipole-exchange spin waves in the magnetic bilayer, the low-loss YIG film should be combined with a magnetic material with lower damping, for instance CoFe ^{41,42} or Heusler alloys⁴³ with an optimized composition.

We now discuss spin-wave reflection at the edge of the YIG/Co bilayer. In the TR-STXM experiments, we imaged

the propagation of spin waves across the bilayer edge while changing the phase of the RF excitation in discrete steps. This allowed us to reconstruct the full process of spin-wave reflection and conversion through the mapping of the entire phase evolution (equivalent to time evolution) of the spin waves. Figure 4(a,c) shows phase-resolved TR-STXM data at 2.36 GHz and a magnetic bias field of -10 mT and $+10$ mT, respectively, which were obtained by averaging the measured 2D maps over the width of the measurement area. Here, the individual line profiles are plotted as a function of the externally controlled phase delay of the RF signal. The dashed line marks the edge of the YIG/Co bilayer. At -10 mT, the spin wave enters the bilayer without a clear phase jump, indicating good transmission across the boundary. For $+10$ mT, the drastic downconversion of the spin-wave wavelength at the bilayer edge does not increase the reflection much, as modulations of the phase signal in the uncovered YIG film caused by wave interference remain small. In case of strong wave reflection, Fig. 4(a,c) would change from a series of sloped lines to a set of vertical lines with abrupt phase jumps (see our previous publication³¹), which is not seen here. We used a simple model^{31,44} to quantitatively analyze the spin-wave reflection coefficient (R). In the model, we assume an incident spin wave A_1 with amplitude A_I in the bare YIG film ($x = 0, \dots, x_{\text{edge}}$) with the initial spin-wave phase offset θ_I being swept between 0 and 2π . The phase of the wave evolves as it travels towards the bilayer as $2\pi \frac{x}{\lambda_1}$. In the same area we further assume a reflected wave A_2 with amplitude A_R now with the initial phase given by the phase of the incident wave at the bilayer edge $\theta_{A_1}(x_{\text{edge}}) = 2\pi \frac{x_{\text{edge}}}{\lambda_1}$. We also add a phase offset $\Delta\theta_R$ stemming from the reflection process. The reflected wave has a negative group velocity and since it is launched from the interface, we write its spatial phase evolution as $2\pi \frac{x_{\text{edge}} - x}{\lambda_1}$. The transmitted wave in the YIG/Co bilayer A_3 has an amplitude A_T and is modeled in the range $x = x_{\text{edge}}, \dots, x_{\text{max}}$. Also here, we assume an initial phase given by the phase of the incident wave A_1 at the bilayer edge and an additional conversion-related phase offset $\Delta\theta_T$. The spatial evolutions of A_1, A_2, A_3 are given by

$$\begin{aligned}
 A_1(x = 0, \dots, x_{\text{edge}}) &= A_I e^{-\frac{x}{l_{d1}}} \cos\left(2\pi \frac{x}{\lambda_1} + \theta_I + \Delta\theta_I\right), \\
 A_2(x = 0, \dots, x_{\text{edge}}) &= A_R e^{-\frac{(x_{\text{edge}} - x)}{l_{d1}}} \cos\left(2\pi \frac{x_{\text{edge}} - x}{\lambda_1} + \theta_{A_1}(x_{\text{edge}}) + \Delta\theta_R\right), \\
 A_3(x = x_{\text{edge}}, \dots, x_{\text{max}}) &= A_T e^{-\frac{(x - x_{\text{edge}})}{l_{d2(3)}}} \cos\left(2\pi \frac{x - x_{\text{edge}}}{\lambda_{2(3)}} + \theta_{A_1}(x_{\text{edge}}) + \Delta\theta_T\right).
 \end{aligned} \tag{1}$$

In these equations, we label the incident and reflected spin waves in the uncovered YIG film as λ_1 , the long-wavelength spin wave in the YIG/Co bilayer (-10 mT) as λ_2 , and the short-wavelength spin wave in the YIG/Co bilayer ($+10$ mT) as λ_3 . Here, $\Delta\theta_I$ is the initial phase offset of the incident spin wave (fixed phase offset/microwave propagation delay for a given RF frequency). To reproduce the experimental data,

we consider spin-wave reflection, transmission, and absorption with coefficients R , T , and D , so that $R + T + D = 1$. If we assume zero absorption during wave conversion, which gives the best result, and omit changes in wave localization and ellipticity, the amplitude of the reflected and transmitted spin waves at the edge of the YIG/Co bilayer can be written as $A_R = RA_I e^{-\frac{x_{edge}}{l_{d1}}}$ and $A_T = (1 - R)A_I e^{-\frac{x_{edge}}{l_{d1}}}$, where $e^{-\frac{x_{edge}}{l_{d1}}}$ is the amplitude if the incident wave. Figure 4(b,d) presents the best fit to the experimental data for ± 10 mT at a frequency of 2.36 GHz. From the calculated spin-wave profiles, we obtain the reflection coefficient at different frequency (Fig. 4(e)). For a bias field of +10 mT, the maximum value of R is about 37% at 1.86 GHz and it reduces to about 12% at 2.36 GHz. A similar dependence is found for -10 mT. Thus, drastic wavelength downconversion is compatible with highly efficient spin-wave transmission, offering a way to generate short-wavelength spin waves in hybrid YIG/FM structures for nanoscale magnonics.

In summary, we imaged efficient downconversion of low-loss dipolar spin waves in YIG ($\lambda = 3.4 - 7.5 \mu\text{m}$) to much shorter dipole-exchange spin waves in a YIG/Co bilayer ($\lambda = 280 - 480$ nm) using TR-STXM. The observed effect, which originates from dynamic dipolar coupling between YIG and Co, opens up an effective way to emit short-wavelength spin waves into hybrid magnonic structures, including waveguides⁴⁵. To enhance the spin-wave decay length ($l_d \approx 4 \mu\text{m}$ in this study), other FM materials with lower magnetic damping should be considered.

I. ACKNOWLEDGEMENT

This work was supported by the Academy of Finland (Grant Nos. 317918, 325480 and 338748). Lithography and FIB milling were performed at the OtaNano-Micronova Nanofabrication Center and the OtaNano-NanoMicroscopy Center, respectively, supported by Aalto University. Computational resources were provided by the Aalto Science-IT project. We thank Helmholtz-Zentrum Berlin for the allocation of synchrotron radiation beamtime.

II. AUTHOR DECLARATIONS

The authors declare no competing interests.

III. AUTHOR CONTRIBUTION

H.J.Q. and S.v.D. led the project. A.T., L.D.Y., and L.F. fabricated and tested the STXM samples. F.S. and S.W. performed the STXM experiments. A.T., H.J.Q. and S.v.D. wrote the manuscript. All authors discussed the results.

IV. DATA AVAILABILITY

The data that support the findings of this study are available from the corresponding authors upon reasonable request.

- ¹A. V. Chumak, V. I. Vasyuchka, A. A. Serga, and B. Hillebrands, "Magnon spintronics," *Nature Physics* **11**, 453–461 (2015).
- ²A. Mahmoud, F. Ciubotaru, F. Vanderveken, A. V. Chumak, S. Hamdioui, C. Adelman, and S. Cotozana, "Introduction to spin wave computing," *Journal of Applied Physics* **128**, 161101 (2020).
- ³A. Barman, G. Gubbiotti, S. Ladak, A. O. Adeyeye, M. Krawczyk, J. Gräfe, C. Adelman, S. Cotozana, A. Naeemi, V. I. Vasyuchka, *et al.*, "The 2021 magnonics roadmap," *Journal of Physics: Condensed Matter* **33**, 413001 (2021).
- ⁴A. Chumak, P. Kabos, M. Wu, C. Abert, C. Adelman, A. Adeyeye, J. Åkerman, F. Aliev, A. Anane, A. Awad, *et al.*, "Advances in magnetics roadmap on spin-wave computing," *IEEE Transactions on Magnetics* **58**, 0800172 (2022).
- ⁵T. Fischer, M. Kewenig, D. Bozhko, A. Serga, I. Syvorotka, F. Ciubotaru, C. Adelman, B. Hillebrands, and A. Chumak, "Experimental prototype of a spin-wave majority gate," *Applied Physics Letters* **110**, 152401 (2017).
- ⁶G. Talmelli, T. Devolder, N. Träger, J. Förster, S. Wintz, M. Weigand, H. Stoll, M. Heyns, G. Schütz, I. P. Radu, J. Gräfe, F. Ciubotaru, and C. Adelman, "Reconfigurable submicrometer spin-wave majority gate with electrical transducers," *Science Advances* **6**, eabb4042 (2020).
- ⁷A. V. Chumak, A. A. Serga, and B. Hillebrands, "Magnon transistor for all-magnon data processing," *Nature Communications* **5**, 1–8 (2014).
- ⁸K. Vogt, F. Y. Fradin, J. E. Pearson, T. Sebastian, S. D. Bader, B. Hillebrands, A. Hoffmann, and H. Schultheiss, "Realization of a spin-wave multiplexer," *Nature Communications* **5**, 1–5 (2014).
- ⁹Q. Wang, P. Pirro, R. Verba, A. Slavin, B. Hillebrands, and A. V. Chumak, "Reconfigurable nanoscale spin-wave directional coupler," *Science Advances* **4**, e1701517 (2018).
- ¹⁰Q. Wang, M. Kewenig, M. Schneider, R. Verba, F. Kohl, B. Heinz, M. Geilen, M. Mohseni, B. Lägel, F. Ciubotaru, C. Adelman, C. Dubs, S. Cotozana, O. Dobrovolskiy, T. Brächer, P. Pirro, and A. Chumak, "A magnonic directional coupler for integrated magnonic half-adders," *Nature Electronics* **3**, 765–774 (2020).
- ¹¹S. Wintz, V. Tiberkevich, M. Weigand, J. Raabe, J. Lindner, A. Erbe, A. Slavin, and J. Fassbender, "Magnetic vortex cores as tunable spin-wave emitters," *Nature Nanotechnology* **11**, 948–953 (2016).
- ¹²B. Van de Wiele, S. J. Hämäläinen, P. Baláz, F. Montoncello, and S. van Dijken, "Tunable short-wavelength spin wave excitation from pinned magnetic domain walls," *Scientific Reports* **6**, 21330 (2016).
- ¹³G. Dieterle, J. Förster, H. Stoll, A. S. Semisalova, S. Finizio, A. Gangwar, M. Weigand, M. Noske, M. Fähnle, I. Bykova, J. Gräfe, D. A. Bozhko, H. Y. Musiienko-Shmarova, V. Tiberkevich, A. N. Slavin, C. H. Back, J. Raabe, G. Schütz, and S. Wintz, "Coherent excitation of heterosymmetric spin waves with ultrashort wavelengths," *Physical Review Letters* **122**, 117202 (2019).
- ¹⁴V. Sluka, T. Schneider, R. A. Gallardo, A. Kákay, M. Weigand, T. Warnatz, R. Mattheis, A. Roldán-Molina, P. Landeros, V. Tiberkevich, A. Slavin, G. Schütz, A. Erbe, A. Deac, J. Lindner, J. Raabe, J. Fassbender, and S. Wintz, "Emission and propagation of 1D and 2D spin waves with nanoscale wavelengths in anisotropic spin textures," *Nature Nanotechnology* **14**, 328–333 (2019).
- ¹⁵L.-J. Chang, J. Chen, D. Qu, L.-Z. Tsai, Y.-F. Liu, M.-Y. Kao, J.-Z. Liang, T.-S. Wu, T.-M. Chuang, H. Yu, and S.-F. Lee, "Spin wave injection and propagation in a magnetic nanochannel from a vortex core," *Nano Letters* **20**, 3140–3146 (2020).
- ¹⁶C. S. Davies, A. V. Sadovnikov, S. V. Grishin, Y. P. Sharaevskii, S. A. Nikitov, and V. V. Kruglyak, "Generation of propagating spin waves from regions of increased dynamic demagnetising field near magnetic antidots," *Applied Physics Letters* **107**, 162401 (2015).
- ¹⁷C. S. Davies and V. V. Kruglyak, "Generation of propagating spin waves from edges of magnetic nanostructures pumped by uniform microwave magnetic field," *IEEE Transactions on Magnetics* **52**, 2300504 (2016).
- ¹⁸J. Stigloher, T. Taniguchi, M. Madami, M. Decker, H. S. Körner, T. Moriyama, G. Gubbiotti, T. Ono, and C. H. Back, "Spin-wave wave-

- length down-conversion at thickness steps,” *Applied Physics Express* **11**, 053002 (2018).
- ¹⁹P. Graczyk, M. Zelent, and M. Krawczyk, “Co- and contra-directional vertical coupling between ferromagnetic layers with grating for short-wavelength spin wave generation,” *New J. Phys.* **20**, 053021 (2018).
- ²⁰S. J. Hämäläinen, F. Brandl, K. J. A. Franke, D. Grundler, and S. van Dijken, “Tunable short-wavelength spin-wave emission and confinement in anisotropy-modulated multiferroic heterostructures,” *Physical Review Applied* **8**, 014020 (2017).
- ²¹S. Klingler, V. Amin, S. Geprägs, K. Ganzhorn, H. Maier-Flaig, M. Althammer, H. Huebl, R. Gross, R. D. McMichael, M. D. Stiles, S. T. B. Goennenwein, and M. Weiler, “Spin-torque excitation of perpendicular standing spin waves in coupled YIG/Co heterostructures,” *Physical Review Letters* **120**, 127201 (2018).
- ²²H. Qin, S. J. Hämäläinen, and S. van Dijken, “Exchange-torque-induced excitation of perpendicular standing spin waves in nanometer-thick YIG films,” *Scientific Reports* **8**, 5755 (2018).
- ²³H. Yu, G. Duerr, R. Huber, M. Bahr, T. Schwarze, F. Brandl, and D. Grundler, “Omnidirectional spin-wave nanograting coupler,” *Nature Communications* **4**, 2702 (2013).
- ²⁴H. Yu, O. D’Allivy Kelly, V. Cros, R. Bernard, P. Bortolotti, A. Anane, F. Brandl, F. Heimbach, and D. Grundler, “Approaching soft X-ray wavelengths in nanomagnet-based microwave technology,” *Nature Communications* **7**, 11255 (2016).
- ²⁵S. Maendl, I. Stasinopoulos, and D. Grundler, “Spin waves with large decay length and few 100 nm wavelengths in thin yttrium iron garnet grown at the wafer scale,” *Applied Physics Letters* **111**, 012403 (2017).
- ²⁶C. Liu, J. Chen, T. Liu, F. Heimbach, H. Yu, Y. Xiao, J. Hu, M. Liu, H. Chang, T. Stueckler, S. Tu, Y. Zhang, Y. Zhang, P. Gao, Z. Liao, D. Yu, K. Xia, N. Lei, W. Zhao, and M. Wu, “Long-distance propagation of short-wavelength spin waves,” *Nature Communications* **9**, 738 (2018).
- ²⁷P. Che, K. Baumgaertl, A. Kúkol’ová, C. Dubs, and D. Grundler, “Efficient wavelength conversion of exchange magnons below 100 nm by magnetic coplanar waveguides,” *Nature Communications* **11**, 1445 (2020).
- ²⁸Y. Au, E. Ahmad, O. Dmytriiev, M. Dvornik, T. Davison, and V. V. Kruglyak, “Resonant microwave-to-spin-wave transducer,” *Applied Physics Letters* **100**, 182404 (2012).
- ²⁹V. V. Kruglyak, “Chiral magnonic resonators: Rediscovering the basic magnetic chirality in magnonics,” *Applied Physics Letters* **119**, 200502 (2021).
- ³⁰J. Chen, T. Yu, C. Liu, T. Liu, M. Madami, K. Shen, J. Zhang, S. Tu, M. S. Alam, K. Xia, M. Wu, G. Gubbiotti, Y. M. Blanter, G. E. W. Bauer, and H. Yu, “Excitation of unidirectional exchange spin waves by a nanoscale magnetic grating,” *Physical Review B* **100**, 104427 (2019).
- ³¹H. Qin, R. B. Holländer, L. Flajšman, F. Hermann, R. Dreyer, G. Woltersdorf, and S. van Dijken, “Nanoscale magnonic Fabry-Pérot resonator for low-loss spin-wave manipulation,” *Nature Communications* **12**, 2293 (2021).
- ³²M. Föhler, S. Frömmel, M. Schneider, B. Pfau, C. M. Günther, M. Hennecke, E. Guehrs, L. Shemilt, D. Mishra, D. Berger, S. Selve, D. Mitin, M. Albrecht, and S. Eisebitt, “A general approach to obtain soft x-ray transparency for thin films grown on bulk substrates,” *Review of Scientific Instruments* **88**, 103701 (2017).
- ³³N. Träger, P. Gruszecki, F. Lisiecki, F. Groß, J. Förster, M. Weigand, H. Glowinski, P. Kuświk, J. Dubowik, M. Krawczyk, *et al.*, “Demonstration of k-vector selective microscopy for nanoscale mapping of higher order spin wave modes,” *Nanoscale* **12**, 17238–17244 (2020).
- ³⁴N. Träger, F. Lisiecki, R. Lawitzki, M. Weigand, H. Glowinski, G. Schütz, G. Schmitz, P. Kuświk, M. Krawczyk, J. Gräfe, *et al.*, “Competing spin wave emission mechanisms revealed by time-resolved x-ray microscopy,” *Phys. Rev. B* **103**, 014430 (2021).
- ³⁵M. Weigand, S. Wintz, J. Gräfe, M. Noske, H. Stoll, B. Van Waeyenberge, and G. Schütz, “TimeMaxyne: A shot-noise limited, time-resolved pump-and-probe acquisition system capable of 50 GHz frequencies for synchrotron-based x-ray microscopy,” *Crystals* **12**, 1029 (2022).
- ³⁶H. Qin, S. J. Hämäläinen, K. Arjas, J. Witteveen, and S. van Dijken, “Propagating spin waves in nanometer-thick yttrium iron garnet films: Dependence on wave vector, magnetic field strength, and angle,” *Physical Review B* **98**, 224422 (2018).
- ³⁷H. Qin, G.-J. Both, S. J. Hämäläinen, L. Yao, and S. van Dijken, “Low-loss yig-based magnonic crystals with large tunable bandgaps,” *Nature Communications* **9**, 5545 (2018).
- ³⁸J. Förster, J. Gräfe, J. Bailey, S. Finizio, N. Träger, F. Groß, S. Mayr, H. Stoll, C. Dubs, O. Surzhenko, N. Liebing, G. Woltersdorf, J. Raabe, M. Weigand, G. Schütz, and S. Wintz, “Direct observation of coherent magnons with suboptical wavelengths in a single-crystalline ferrimagnetic insulator,” *Physical Review B* **100**, 214416 (2019).
- ³⁹P. Grünberg, “Magnetostatic spin-wave modes of a heterogeneous ferromagnetic double layer,” *Journal of Applied Physics* **52**, 6824–6829 (1981).
- ⁴⁰B. A. Kalinikos and A. N. Slavin, “Theory of dipole-exchange spin wave spectrum for ferromagnetic films with mixed exchange boundary conditions,” *Journal of Physics C: Solid State Physics* **19**, 7013 (1986).
- ⁴¹M. A. W. Schoen, D. Thonig, M. L. Schneider, T. J. Silva, H. T. Nembach, O. Eriksson, O. Karis, and J. M. Shaw, “Ultra-low magnetic damping of a metallic ferromagnet,” *Nature Physics* **12**, 839–842 (2016).
- ⁴²L. Flacke, L. Liensberger, M. Althammer, H. Huebl, S. Geprägs, K. Schultheiss, A. Buzdakov, T. Hula, H. Schultheiss, E. R. J. Edwards, H. T. Nembach, J. M. Shaw, R. Gross, and M. Weiler, “High spin-wave propagation length consistent with low damping in a metallic ferromagnet,” *Applied Physics Letters* **115**, 122402 (2019).
- ⁴³C. Guillemard, S. Petit-Watelot, L. Pasquier, D. Pierre, J. Ghanbaja, J.-C. Rojas-Sánchez, A. Bataille, J. Rault, P. Le Fèvre, F. Bertran, and S. Andrieu, “Ultralow magnetic damping in Co₂Mn-based Heusler compounds: Promising materials for spintronics,” *Physical Review Applied* **11**, 064009 (2019).
- ⁴⁴R. Verba, V. Tiberkevich, and A. Slavin, “Spin-wave transmission through an internal boundary: Beyond the scalar approximation,” *Physical Review B* **101**, 144430 (2020).
- ⁴⁵H. Qin, R. B. Holländer, L. Flajšman, and S. van Dijken, “Low-loss nanoscopic spin-wave guiding in continuous yttrium iron garnet films,” *Nano Letters* **22**, 5294–5300 (2022).